Single-Molecule Nanosecond Anisotropy Dynamics of Tethered Protein Motions

Dehong Hu and H. Peter Lu*

Pacific Northwest National Laboratory, Fundamental Science Division, P.O. Box 999, Richland, Washington 99352

Received: June 6, 2002; In Final Form: August 21, 2002

Confined and hindered protein motions generally exist in living cells, with tethered proteins or protein domains particularly associated with and relevant to the early events of molecular interactions in cell signaling at extra- and intracellular membrane surfaces. Ensemble-averaged, time-resolved fluorescence anisotropy has been extensively applied to study the protein rotational and conformational motion dynamics under physiologically relevant conditions. However, the spatial and temporal inhomogeneities of the nonsynchronizable stochastic protein rotational and conformational motions are extremely difficult to characterize with such ensemble-averaged measurements. Here, we demonstrate the use of single-molecule nanosecond anisotropy to study the tethered protein motion of a T4 lysozyme molecule on a biologically compatible surface under water. The rotational motions of tethered proteins are confined in a half-sphere whose volume is primarily defined by the linker and the surface. We observe dynamic inhomogeneities of the rotational diffusion dynamics, i.e., diffusion rate fluctuation, because of interactions between the proteins and the surface. However, we also find that the long-time averages of the dynamically inhomogeneous diffusion rates of single molecules are essentially homogeneous among the single molecules examined. Moreover, tethered proteins stay predominately in solution, rather than being fixed on the modified surface. The infrequent surface interactions are not energetic enough to fix the protein rotational motions. These results suggest that the motions of proteins tethered to surfaces are dynamically inhomogeneous, even if the surfaces or the local environments are homogeneous; in contrast, static inhomogeneity of the rotation dynamics can only exist when the local surface or the local environment are inhomogeneous. Furthermore, the tethered-proteins are found to be in solution without rotational rate fluctuations for most of the time during the measurements, suggesting that the use of tethered proteins on modified glass surfaces under water is a reasonable way to study protein dynamics in solution, as many single-molecule experiments have demonstrated. Our approach allows the recording of time trajectories of the single-molecule rotation rate fluctuation and reveals the single-molecule rotational motion over wide time scale from subnanoseconds to seconds.

Introduction

Proteins in living cells are often spatially confined and hindered in diffusion because of their covalent or noncovalent interactions with the cell membrane, mitochondrion, and other cellular structural components. Tethered protein diffusion motions in living cells are associated with many important cellular processes, such as cell signaling, DNA−protein and protein−protein interactions, and molecular recognition. The translational, rotational, and conformational motions of the proteins are often confined and inhomogeneous, and the inhomogeneity can be both static and dynamic. Static and dynamic inhomogeneities of rate processes are due to the different local environments of single molecules and their couplings to fluctuating local environments, respectively.[1] Although dynamic inhomogeneity often holds the critical molecule-level understanding of the protein dynamics and mechanism, it is extremely difficult, if not impossible, to characterize in an ensemble-averaged experiment.[2] Inhomogeneity can be better identified and characterized by single-molecule spectroscopy, studying one molecule at a time and analyzing the time trajectory of a single-molecule rate constant with high time-resolution. It has been well-known that many crucial protein motions occur on the picosecond to nanosecond time scales.[3,4] A few recent single-molecule spectroscopic studies[2,5−17] have demonstrated the significant advantage of studying the inhomogeneity of protein dynamics by monitoring single-molecule time trajectories accompanied with statistical analysis of the time trajectories. However, the time resolution achieved to date has been in milliseconds.

The use of single-molecule polarization anisotropy is advantageous in probing rotational dynamics and structural ordering. Primarily two types of single-molecule anisotropy methods have been demonstrated. One type uses either polarized excitation or polarized emission to record a time trace of the steady-state polarization anisotropy or the orientation of the transition dipole.[18−37] This approach is often used to study the rotation dynamics in the millisecond time regime for spatially confined or fixed single molecules. The time resolution of the trajectory is usually in milliseconds, limited by the photon emission rate. A second type[38] studies the free diffusion of single molecules in solution by time-correlated single photon counting (TCSPC), resolving single-molecule rotation dynamics with subnanosecond time resolution by analyzing a photon burst from a single molecule as it diffuses through the laser focal volume. However, in this method, the time trajectory of the anisotropy is not recorded for the single molecule because of the limited number

* To whom correspondence should be addressed. E-mail: peter.lu@pnl.gov.

10.1021/jp0213654 CCC: $25.00
Published on Web 12/05/2002

of photons detected from the molecule. In this paper, we report on a new approach that combines the advantages of both the subnanosecond time resolution of TCSPC and the ability for single-molecule time trajectory recording. This work extends current single-molecule anisotropy studies by analyzing the rotation dynamics of tethered proteins using a photon time-stamping TCSPC apparatus, based on techniques previously reported.[39,40] Using this new approach, we were able to study dynamics over a wide range of time scales, both the nanosecond fast dynamics and the submillisecond or longer slow dynamics.

We report findings about rotational motion dynamics of tethered T4 lysozyme proteins on a hydrocarbon-modified glass surface under water, a model environment of extra- and intracellular membrane surfaces. A major obstacle for previous methods has been the coupling of fluorescence lifetime fluctuations[1] into the single-molecule anisotropy dynamics data, a kind of "contamination" that makes data analysis extremely difficult, if not impossible. There are many reasons for fluorescence lifetime fluctuation, such as quenching by oxygen or local environment fluctuations, which are not necessarily related to the protein rotational motions.[1] In contrast, our approach can effectively distinguish and selectively measure rotational motion dynamics without the "contamination" of fluorescence lifetime fluctuation.

The Alexa 488 labeled wild-type T4 lysozyme has been chosen as a model system because of its accessibility to covalent and site-specific dye-labeling, well characterized static structure, cell-wall associated catalytic function, and feasible fluorescence imaging and spectroscopy at the single-molecule level.[5] Immobilized single T4 lysozyme proteins on a hydrocarbon-treated glass surface by a covalent bifunctional linker allows recording of long fluorescence intensity and lifetime trajectories limited only by photobleaching. Both a millisecond anisotropy trajectory and nanosecond anisotropy decay rate constants were measured at the same time for a single molecule using our new approach.

Experimental Section

The wild-type T4 lysozyme[41] has two cystein groups, Cys54 and Cys97, which are accessible to dye labeling through thiolation. The cystein group of the enzyme was labeled by Alexa 488 maleimide (Molecular Probes) by the standard protocol from Molecular Probes. The reaction yield is controlled to be low to ensure the doubling labeling is insignificant. The product was purified by gel filtration with a Sephadex G25 column to separate unreacted Alexa 488 from the protein. The dye Alexa 488 may be attached either to Cys54 or Cys97. An *Escherichia coli B* cell wall assay[5] showed that the enzyme remains active after labeling. The labeled enzyme was then immobilized by tethering through a covalent linker molecule on a glass coverslip surface. Coverslips were first derivatized with a 10% (v/v) mixture of 3-mercaptopropyl-trimethoxysilane and isobutyltrimethoxysilane ($1{:}10^4$ ratio) in DMSO for 24 h. After washing with methanol and PBS buffer, coverslips were incubated in 10 nM of SIAXX (Molecular Probes, S-1668) in PBS buffer pH 7.2 for 1 h. After washing, the coverslips were incubated with 1 nM of protein in 0.2 M of carbonate buffer, pH 8.2, for 1 h followed by rinsing with PBS buffer. To simulate the biologically relevant environment, we further modified the hydrophobic surface by adding 60 nM nonlabeled wild-type T4 lysozyme proteins in the solution, which typically results in coverage of those surface defect-sites that strongly interact with and adsorb T4 lysozyme molecules. We also made rhodamine 123 single-molecule samples by spin-coating 3×10^{-10} M rhodamine 123 in methanol in thin PMMA film on glass coverslips as the control experiment of the single-molecule anisotropy.

A confocal microscope with a focused laser was used to locate the individual protein molecules and measure the single-molecule fluorescence intensity trajectories. The output of the Coherent MIRA900 fs laser at a 950-nm wavelength and 75.7-MHz repetition rate was frequency-doubled and coupled through a single-mode optical fiber. The beam was collimated after the fiber and passed through a polarizer, and the excitation light was attenuated to $0.1\sim1$ μW. The beam was sent into the microscope from its epi-port, reflected up by a dichroic beam-splitter (Chroma 505DCLP), and focused by a $100\times$ oil immersion objective lens (Zeiss Fluar NA 1.3) onto the upper sample surface of a microscope coverslip (Fisher Scientific, 0.17 mm thick). The waist of the input excitation beam was adjusted to be smaller than the size of the back aperture of the objective lens to compromise between high resolution and maintenance of in-plane polarization at the focal point. The sample can be raster-scanned or moved to a particular position with respect to the laser focus using an x-y electro-piezo close-loop position scanning stage (Physik Instrumente). The fluorescence was collected by the same objective lens and was directed to the camera port of the microscope after going through the dichroic beam-splitter. The scattered excitation light was cut off by a colored glass long-pass filter (HQ515LP). The fluorescence signal was split by a polarizing beam-splitter so that the two beams detected were the parallel and perpendicular components of the fluorescence. The two-channel signals were imaged onto a pair of photon-counting detectors, either avalanche photodiodes (APD; Perkin-Elmer, SPCM-AQR-16 and SPCM-AQ-151) or PMT (Hamamatsu H7522-40). The small active area of the APD (200 μm diameter) and a pinhole in front of the PMT ensured confocal imaging. All measurements were conducted under ambient conditions.

The detection electronics were derived from typical time-correlated single-photon counting (Figure 1). The two APD signals were directly sent to two time-to-amplitude converters (TAC) (Canberra, model 2145) as a "start" signal. If the PMT instead of the APD were used, the PMT signals went through preamplifiers and constant fraction discriminators before being sent to the TAC "start". The photodiode signal from Mira 900 was used as a "stop" signal for the TAC. The two TAC outputs were sent to a homemade two-channel digitizer instead of to a multichannel analyzer. The digitizer recorded each pulse's amplitude and arrival time with the resolution of 0.1 μs. A recorded trajectory usually contained hundreds of thousand of photons. For each photon, the detector identification, arrival time, and TAC amplitude, which corresponds to the delay time between laser excitation pulse and detected photon in nanoseconds or picoseconds, were stored in the computer for future data analysis. The functionality of our homemade data recording electronics and computer interfacing system is similar to "burst-integrated fluorescence lifetime" and "time-tagged time-resolved"systems.[39,40] The instrument response function (IRF) is measured by the reflection of excitation light from the sample after removing the colored glass long pass filter. The photon time-stamping TCSPC can measure the anisotropy dynamics both in a slow time range (from submilliseconds to seconds) and a fast time range (from subnanoseconds to nanoseconds). The slow time range is limited by the single-molecule emission rate and by photobleaching; the fast time range is limited by detection IRF and the single-molecule fluorescence lifetime.

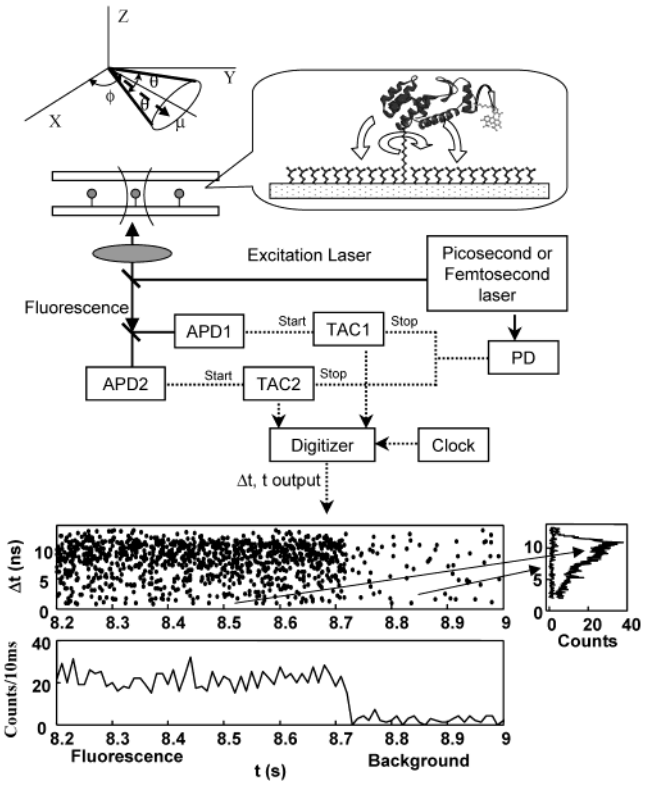

Figure 1. Schematic of a single-molecule confocal microscope with two-channel photon time-stamping TCSPC. It allows us to study the fluorescence intensity, lifetime, and anisotropy of a single molecule simultaneously by recording the arrival time and delay time of each fluorescence photon. The top-left plot is an example of the raw data of the photon time-stamping TCSPC of a detector channel. Each dot corresponds to a photon detected plotted by its arrival time (t) and delay time (Δt) (raw output from TAC in reverse timing). The fluorescence intensity trajectory (bottom plot) is calculated from the histogram of arrival time (t) with 0.01 s time-bin resolution. The molecule was photobleached at 8.71 s. The nanosecond fluorescence decay curves (top-right plot) are the histograms of the delay time of the fluorescence photons (t < 8.71 s) and background photons (t > 8.71 s).

Results

Fitting Time-Resolved Anisotropy. The analysis of time-resolved fluorescence anisotropy decay of solution phase free rotating molecules has been extensively discussed.[42−44] Here we use the well-developed fitting method to analyze the anisotropy decay of tethered T4 lysozyme although its rotation might be restricted. The observed parallel and perpendicular intensities have some cross-talk from $I_{||}(t)$ and $I_{\perp}(t)$ because of the collection of Z-polarized light by objective. However, Z orientated single molecules have lower intensities and are often ignored because both the excitation rate and detection efficiency are low. Furthermore, we expect that the tethered protein mainly has the rotation in $X-Y$ plane. So the effect of Z polarized light is not included in the data analysis. The observed weighting-factor-corrected emission curves $I_{||}(t)$ and $I_{\perp}(t)$ are the convolution of instrument response function IRF(t) and the true decay functions $i_{||}(t)$ and $i_{\perp}(t)$:

$$I_{||}(t) = i_{||}(t) \otimes IRF(t)$$

$$I_{\perp}(t) = i_{\perp}(t) \otimes IRF(t)$$

To simplify data analysis, we assume the excited-state population decay and the anisotropy decay as single-exponential functions with lifetime of τ and ρ, with preexponential factors A and α, respectively:

$$i_{||}(t) = A \exp\left(-\frac{t}{\tau}\right)\left[1 + 2\alpha \exp\left(-\frac{t}{\rho}\right)\right]$$

$$i_{\perp}(t) = A \exp\left(-\frac{t}{\tau}\right)\left[1 - \alpha \exp\left(-\frac{t}{\rho}\right)\right]$$

Thus

$$I_{||}(t) + 2I_{\perp}(t) = 3A \exp\left(-\frac{t}{\tau}\right) \otimes IRF(t)$$

$$I_{||}(t) - I_{\perp}(t) = 3A\alpha \exp\left[-\left(\frac{1}{\tau} + \frac{1}{\rho}\right)t\right] \otimes IRF(t)$$

First, the data of the pure fluorescence decay, $I_{||}(t) + 2I_{\perp}(t)$, were fit to get A and τ by nonlinear least-squares or maximum likelihood estimation fitting routine.[45] Then, we fit the data of $I_{||}(t) - I_{\perp}(t)$ to get $A\alpha$ and $(1/\tau + 1/\rho)$. The anisotropy decay parameters then could be calculated. This analysis requires that the two detectors have identical instrument-response functions. This requirement can be easily satisfied in ensemble-averaged measurements because parallel and perpendicular fluorescence intensities are measured with same detector and different polarizer angles. In single-molecule measurements, to achieve maximum detection efficiency, two detectors with fixed polarizing beam-splitter are usually used. If two detectors have different instrument response functions, the experimental curves must be fitted individually. Single exponential fittings are used here since biexponential fits do not give better fitting because of the signal-to-noise level in our single-molecule experiments. To resolve multiexponential decay of a single-molecule anisotropy, more than approximately 10^6 detected photons have to be recorded, as in typical TCSPC bulk samples. That number is often precluded by photobleaching in single molecule measurements. Here we use empirical formulas for the two detector signals $I_{||}(t)$ and $I_{\perp}(t)$ with parameters A_1, A_2, τ_1, and τ_2

$$i_{||}(t) = A_1 \exp\left(-\frac{t}{\tau_1}\right)$$

$$i_{\perp}(t) = A_2 \exp\left(-\frac{t}{\tau_2}\right)$$

$$I_{||}(t) = A_1 \exp\left(-\frac{t}{\tau_1}\right) \otimes IRF_1(t)$$

$$I_{\perp}(t) = A_2 \exp\left(-\frac{t}{\tau_2}\right) \otimes IRF_2(t)$$

Thus, we get parameters A_1, A_2, τ_1, and τ_2 from decay curve fitting. However, the model anisotropy decay $r(t)$ is not a single-exponential decay:

$$r(t) = \frac{i_{||}(t) - i_{\perp}(t)}{i_{||}(t) + 2i_{\perp}(t)} = \frac{A_1 \exp(-t/\tau_1) - A_2 \exp(-t/\tau_2)}{A_1 \exp(-t/\tau_1) + 2A_2 \exp(-t/\tau_2)}$$

It has a large deviation from the true anisotropy decay at large t, because both parallel and perpendicular intensities are very small and produce a very unstable value of anisotropy. In contrast, at small t, the $r(t)$ presents the true anisotropy decay precisely. By assuming that the model decay $r(t)$ and the true

decay $\alpha \exp(-t/\rho)$ have the same value and first derivative at $t = 0$, we can calculate α and ρ from A_1, A_2, τ_1, and τ_2:

$$\alpha = \frac{A_1 - A_2}{A_1 + 2A_2} \quad (1)$$

$$\rho = \frac{\tau_1\tau_2(2A_2^2 - A_1A_2 - A_1^2)}{3A_1A_2(\tau_1 - \tau_2)} \quad (2)$$

An alternative way to calculate ρ is based on the relation between steady-state anisotropy R and α

$$R = \frac{\alpha\rho}{\rho + \tau}$$

R is calculated from steady-state data. α is calculated from eq 1. τ is calculated by averaging τ_1 and τ_2 by weight A_1 and $2A_2$. Then, ρ can be calculated from the above equation, and the result is

$$\rho = \frac{2A_2^2\tau_2^2 - A_1A_2\tau_1\tau_2 - A_1^2\tau_1^2}{3A_1A_2(\tau_1 - \tau_2)} \quad (3)$$

Equation 2 has advantages for restricted rotations. Although eqs 2 and 3 have a different mathematical form, they give similar results from the experimental data of single T4 lysozyme molecules.

By comparing both fitting methods from the same data set from our T4 lysozyme labeled with Alexa 488, we found that the difference in α and ρ resulting from the fitting is small (3% error of α and 0.02 ns^{-1} error of $1/\rho$).

Fitting of the exponential decay has both random errors and systematic errors. Photon shot noise is the major source of the random error. For a single exponential decay, the lifetime can be estimated by the average of photon delay time assuming a Poisson photon detection process. The relative standard deviation of this estimation reduces with the square root of the number of total photons. In data analysis, the fitted lifetimes have typically larger errors because of the instability of the convolution fitting and slow IRF. To test our single-molecule data quality, we separated photons into 10 groups and compared the fitting results from each group. For a typical single molecule with total 3×10^4 photons recorded, each group contains 3×10^3 photons. The results gave fitted lifetimes with a relative standard deviation of 6% and an amplitude standard deviation of 3%. Therefore, we estimate that the fitting of all photons has a lifetime random error of 2% and an amplitude random error of 1% because of the limited number of photons. Other random errors from the instability of laser and electronics are minimal. On the other hand, systematic errors in the decay curve fitting are caused by electronic and optical reflections, unmatching IRF with real data, etc. These systematic errors typically exist in the standard TCSPC, as well. We estimate the total systematic error to be less than 5%.

Modeling the Restricted Rotation of a Transition Dipole. The rotation of Alexa 488 dye tethered on a T4 lysozyme is a complicated process involving multiaxis multibody restricted rotation. To simplify the calculation, we here calculate only the restricted rotation of a transition along a single axis to model the motion of a T4 lysozyme, assuming that the T4 lysozyme only has one rotation axis normal to the surface. The mean orientation angle relative to the laboratory frame is ϕ and the range is from $\phi - \theta$ to $\phi + \theta$ (Figure 1). The probability distribution of ω is chosen to be

$$P(\omega) = (1 + \cos(\pi(\omega - \phi)/\theta))/(2\pi)$$

to simulate a wave function of rotation. Therefore, the parallel and perpendicular intensities at time zero are

$$i_{||}(0) = \int_{\phi-\theta}^{\phi+\theta} \cos^4(\omega)\, P(\omega)\, d\omega$$

$$i_{\perp}(0) = \int_{\phi-\theta}^{\phi+\theta} \cos^2(\omega) \sin^2(\omega)\, P(\omega)\, d\omega$$

The time-zero anisotropy is

$$\alpha(\phi,\theta) = \frac{i_{||}(0) - i_{\perp}(0)}{i_{||}(0) + 2i_{\perp}(0)}$$

Assuming the distribution of ϕ is uniform, the average anisotropy is

$$\langle\alpha\rangle = \frac{1}{\pi}\int_0^{\pi} \alpha(\phi, \theta) d\phi$$

which is a function of θ. This function is evaluated numerically and plotted in Figure 2.

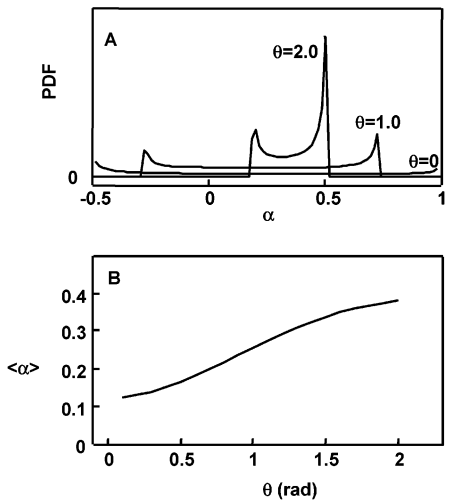

Figure 2. Simulation of wobbling-angle dependent anisotropy. (A) The probability density function of time-zero anisotropy with different restriction angles (0, 1.0, and 2.0 rad). (B) The average time-zero anisotropy vs the restriction angle θ. The average time-zero anisotropy for no restriction ($\theta \rightarrow \infty$) is 0.4.

On the basis of the assumption of uniform distribution of ϕ, the distribution of α is also plotted in Figure 2 with θ as a parameter. As we can see, a smaller θ gives a smaller average α and a wider α distribution. If $\theta = 0$ (corresponding to the situation if the transition dipole is fixed), the α distribution is from -0.5 to 1 and $\langle\alpha\rangle = 0.121$. We note here that $\langle\alpha\rangle$ is different from the anisotropy of fixed transition dipoles in the ensemble measurement, which is 0.4, because of the difference in the definition of anisotropy. In an ensemble measurement, the parallel and perpendicular fluorescence of all transition dipoles are summed before calculating α. Here, we calculate α for each transition dipole and then calculate the average of α. If the rotation of the transition dipole has no restriction, the α distribution is a delta function at 0.4, which is a special case of the above analysis.

Data Analysis. For aqueous samples, the water Raman signal contributes the majority of the background intensity, as shown

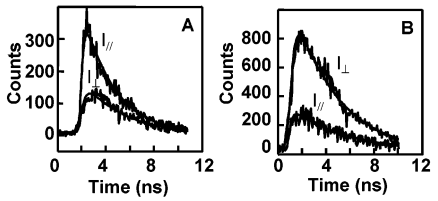

Figure 3. Parallel and perpendicular fluorescence decay and single exponential fits of a single T4 lysozyme/Alexa 488 molecule covalently linked to surface (A) and a single rhodamine 123 molecule on PMMA surface (B). The decay curves are integrated from all detected photons of parallel and perpendicular channels before photobleaching.

in the spectrum of the background. It produces an instrument response function (IRF) limited spike in the parallel channel. The additional background may come from the fluorescence of color filters, objective oil, or other optical components. This background has a broad spectrum and slow decay dynamics (>10 ns), and it occurs in both aqueous samples and dry samples. However, this background intensity is typically very small (~1/30) compared to single-molecule fluorescence intensity. The background signal from elastically scattered excitation light is completely blocked by filters and is not measurable.

The photon time-stamping TCSPC data contain more nonscrambled, detailed information than a conventional TCSPC histogram, adding a delay-time trajectory, i.e., the consecutive delay times between the excitation pulse and each emitted photon, and the arrival-time trajectory, i.e., the consecutive arrival time of each detected photon. The data can be used to analyze the single-molecule dynamics not only from microsecond to second time scales but also from picosecond and nanosecond time scales. Two nanosecond TCSPC histograms were calculated: the single-molecule signal of all of the fluorescence photons detected plus background before photobleaching and the background after photobleaching (Figure 1). Both the parallel and perpendicular single-molecule nanosecond decay histograms were calculated by subtracting the corresponding background histogram from the signal histogram. Figure 3A shows the fitting of parallel and perpendicular decays of a typical single molecule. The anisotropy decay time and amplitude were then calculated, based on the method in the previous section. Seidel et al. have studied the time-resolved nanosecond anisotropy decay of freely diffusing single molecules in solution.[38] Each burst of fluorescence intensity corresponds to a single molecule. The time-resolved anisotropy decay was analyzed from parallel and perpendicular fluorescence decays. In this work, we study one molecule at a time selectively. The integration time is longer, and more photons are recorded from the individual molecule examined. Consequently, the signal-to-noise ratio (S/N) of our method is about 10 times higher. We are not only able to measure the nanosecond anisotropy decay but also record the trajectory of the anisotropy amplitude and the decay constant from an individual molecule.

We were able to measure the time-resolved anisotropy decay time (ρ) and time-zero amplitude (α) fluctuation trajectories without the contamination of fluorescence lifetime fluctuations. To reach a higher time-resolution, the fluorescence decay histogram can also be calculated based on the photons within a short time period, for example, 0.2 s. Then, the fluorescence lifetime and anisotropy decay time can be calculated for this period. Therefore, the ρ and α are shown as a trajectory (Figure 4 parts A and B for a typical molecule, lifetime trajectory not shown) for the whole life of the single molecule before photobleaching. This time-resolved anisotropy trajectory provides more information about the fast dynamics than does the

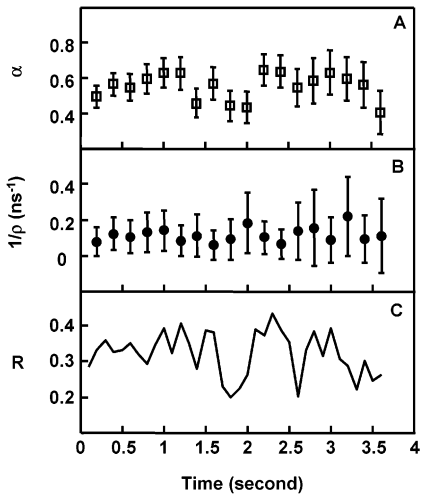

Figure 4. Anisotropy trajectory of a T4 lysozyme single molecule. The time-zero anisotropy amplitude α (top) and anisotropy decay rate constant $1/\rho$ (middle) are calculated by fitting the parallel and perpendicular decay curves from photons in 0.2 s time-bin resolution. The error bars ($\pm$ one sigma) of the top and middle plots are estimated by the random error of fitting, based on the number of photons in the fitting and error propagation through eqs 1 and 2. The steady-state anisotropy *R* (bottom) is calculated from the parallel and perpendicular fluorescence intensity with 0.1 s time-bin resolution. Although the steady-state anisotropy trajectories of the single molecules often show fluctuation at sub-second time scale, this fluctuation is not pure rotational dynamics due to the coupled fluorescence lifetime fluctuation.

steady-state anisotropy (*R*) trajectory (Figure 4C). This novel nanosecond rate constant fluctuation with subsecond resolution trajectory provides pure anisotropy dynamics and insight information about the conformational dynamics. Presumably, if the fluorescence lifetime is constant, the steady-state anisotropy (*R*) is related to ρ and α. However, single-molecule fluorescence fluctuation is typically significant, and the decoupling of the lifetime fluctuation from the steady-state anisotropy is very difficult. The fluorescence lifetime of the single molecule in Figure 4 fluctuates in the range of 2.8 ± 0.4ns. The fluorescence lifetime of all single molecules that we studied has a distribution width of 0.3 ns. The fluctuation trajectory of *R* (Figure 4C) is evidentially different from the trajectory of time-zero anisotropy amplitude because the *R* fluctuation results from a convoluted contribution of fluorescence lifetime fluctuation, rotational time (ρ) fluctuation, and time-zero anisotropy amplitude (α) fluctuation. There are many reasons for lifetime fluctuation not to be related to protein rotation, e.g., quenching. Such "contamination" is a major obstacle for rotation-dynamics measurements of single molecules in an inhomogeneous environment, such as proteins in living cells, which makes measurements less relevant and inaccurate. The direct measurement of ρ and α gives pure anisotropy dynamics without the fluorescence lifetime fluctuation "contamination."

The reflected excitation laser from the sample surface was used to measure instrument response function. The anisotropy decay time and amplitude were calculated from the fitting of parallel and perpendicular decay curves. More than 100 molecules of T4 lysozyme, labeled with Alexa 488, with enough photons for fitting to give a reasonably precise amplitude and lifetime among all molecules, are analyzed and their anisotropy decay results summarized in Figure 5.

The first moment of the single-photon delay time distribution is also used to determine the decay lifetime of a single molecule as a Poisson distribution of the delay time. In reality, the delay

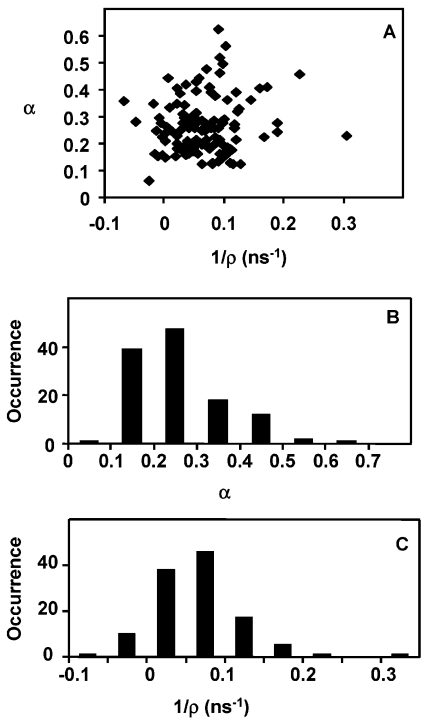

Figure 5. (A) Correlation between time-zero anisotropy (α) and anisotropy decay rate (1/ρ) of single tethered T4 lysozyme molecules. (B) The histogram of the time-zero anisotropy values. (C) The histogram of the of anisotropy decay rates. The time-zero anisotropy and decay rate constant are calculated from all detected photons from each molecule.

time distribution is an exponential distribution convoluted with IRF. However, the convolution operation of IRF adds only a constant to the mean decay time of the original function, and because this constant does not fluctuate, it does not contribute to the fluctuation dynamics of the decay time (Figure 4).

Control Experiments. We have measured the steady-state anisotropy and the time-zero anisotropy of the dye molecules on polymer and in solution. To show the difference in the anisotropy of rotating and fixed molecules, we made rhodamine 123 single-molecule samples by spin-coating 3×10^{-10} M rhodamine 123 in methanol on thin PMMA film on a glass coverslip. It is known that most single dye molecules at air/polymer interface are fixed and rarely show rotation jumps except some dyes show wide range of rotation dynamics.[1,25,37,46]

We also measured the time-zero anisotropy of Alexa 488 dye in solution. All optics and electronics have been the same as for single-molecule measurements, except the excitation focal point is inside a droplet of 1×10^{-7} M solution. Because the rotation time of Alexa 488 in water was too short to be resolved by our instrument, we used glycerol as a solvent for Alexa 488 to measure its time-zero anisotropy, and the result is 0.31 ± 0.03. The error is estimated mainly from the imperfectness of the optical polarization.

The anisotropy decay of Alexa 488 labeled T4 lysozyme in buffer solution has two components decaying at different rates. The decay time of the fast component is instrument-response-function limited (500 ps), and we attribute this fast decay rate constant to the wobbling of the Alexa 488 probe. The slow anisotropy component has an amplitude of about 0.18 ± 0.04. The error is mainly from the dye labeling reaction and incomplete separation of unreacted dye. The decay time, ~10 ns, is attributed to the rotation of the T4 lysozyme. The extent of the restricted motion is described by the order parameter S^2:

$$S^2 = \frac{r(0^+)}{r(0)}$$

where $r(0)$ is the true initial anisotropy and $r(0^+)$ is the extrapolation of the slow anisotropy decay back to time zero.[47] If we consider that the total anisotropy amplitude including the unresolved fast component is 0.31, the order parameter for the protein rotation is 0.6. The Alexa 488 probe has the wobbling motion, which is restricted but not completely fixed by the protein. The order parameter shows the freedom of the probe's wobbling on the protein. This result essentially agrees with the literature data of egg lysozyme with eosin that also has two anisotropy decay components, a fast one due to the wobbling of the dye and a slow one due to the rotation of the protein. The protein rotation has a decay time of 7 ns and an order parameter of 0.78.[47] The difference in the order parameter may come from the sample purity, the size of the dye, or local conformation of the different lysozymes. The slow anisotropy decay component in the ensemble measurement is also observed in the single-molecule measurement. The IRF limited fast component from the dye wobbling motion is not observed in single-molecule spectroscopy because of the limited number of photons. We note that the anisotropy decay time of the bulk has less error than that of single molecules because the bulk measurement has a better signal-to-noise ratio. The bulk anisotropy decay time is beyond error and clearly shows that the T4 lysozyme in buffer solution has rotation dynamics. The interpretation of single molecule anisotropy decay time will be discussed in detail later.

The efficiencies of two detection channels (Figure 3) were not balanced, primarily because of the difference of the quantum efficiencies of the two APD detectors and the bias of the dichroic beam splitter, mirrors, and the polarizing beam splitter. Here, we used the weighting factor to correct the imbalance of the two detection channels. Fluorescence spheres (Molecular Probes, 500 nm yellow-green spheres) are used to measure the weighting factor. We first chose the excitation polarization parallel to detector 1 and measured the fluorescence intensity of a sphere on the two detectors, I_{11} and I_{12}. We then used excitation polarization parallel to detector 2 and measured the fluorescence intensities I_{21} and I_{22} of the same sphere on detectors 1 and 2. The weighting factor is $((I_{11}I_{21})/(I_{12}I_{22}))^{1/2}$, and the error of the weighting factor was estimated as ~5%. The measured weighting factor, typically between 0.9 and 1.1, was used to compensate the measured signals from the two detectors in single-molecule time-resolved anisotropy experiments under the same measurement conditions.

The ensemble-averaged anisotropy of Alexa 488 labeled T4 lysozyme tethered on a surface was analyzed by a control experiment. The sample was prepared by introducing a high fraction of the functional group for tethering: a $1{:}10^2$ ratio of 3-mercaptopropyl-trimethoxysilane and isobutyltrimethoxysilane. The other conditions were the same as described in the Experimental Section. The parallel and perpendicular fluorescence intensities were obtained by scanning a 50×50 μm^2 sample area at 4 ms per pixel rate and 0.5 μm per pixel spatial resolution. The ensemble-averaged time-zero anisotropy of tethered T4 lysozyme was found to be 0.18 ± 0.03. The measurements of tethered T4 lysozyme and T4 lysozyme in buffer solution have the same source of error.

Discussion

We were able to probe the inhomogeneity of the tethered protein rotation dynamics by identifying each molecule's

anisotropy amplitude and rate constant. The tethered proteins were found to remain in solution phase with nearly free rotation. The parallel and perpendicular fluorescence decays of single molecules were fitted, and their anisotropy results are shown in Figure 5. The time-zero amplitude (α) distribution of the anisotropy of single T4 lysozyme proteins with Alexa 488 is shown in Figure 5A; the averaged single-molecule anisotropy amplitude $\langle\alpha\rangle$ of the protein motion is 0.23 ± 0.04. (Besides the fitting errors discussed, incomplete sampling of the ensemble may also contribute to the error.) Further results of the anisotropy for the tethered protein motion from the 2-D scanning ensemble-averaged measurement is also consistent with the results of single molecule measurements. The measured anisotropy decay rate, $1/\rho$, of tethered T4 lysozyme has a broad distribution (Figure 5B). To interpret its rotation rate, both systematic and random errors of the anisotropy decay rate have to be considered. Molecules with decay rate constants larger than 0.1 ns^{-1} were interpreted as preserving a fast rotation as in solution. A significant fraction of molecules have decay rates smaller than 0.1 ns^{-1}; however, because the fluorescence lifetime decay constant of 0.38 ns^{-1} is much larger than the anisotropy decay rate constant, the slow rotation or nonrotation cannot be differentiated because of the uncertainty of the fitting, which sometimes even gives negative-fitted decay rate constants.

To further study the anisotropy of tethered T4 lysozyme molecules, we analyzed the fluorescence intensity trajectories from the arrival times of each photon, especially those molecules with a rate constant of anisotropy decay smaller than 0.1 ns^{-1}. In general, there are three possibilities:[18,30] (1) the molecular rotational motions are fixed; (2) the molecules rotate at the time scale comparable to the single-molecule trajectory recording time limited by photobleaching, i.e., milliseconds to seconds; or (3) the molecules rotate faster than the dwell time of the intensity trajectory, i.e., typically milliseconds, based on the emission rate to get enough counts to measure intensity, but slower than fluorescence lifetime (2.6 ns in aqueous solution).[18,30] If the molecule rotates at the milliseconds to seconds time scale, the slow rotation of the transition dipole should cause an anticorrelated fluctuation of the parallel and perpendicular fluorescence intensity. Instead, the parallel and perpendicular intensity trajectories show essentially correlated fluctuation because of single-molecule fluorescence "blinking". The cross-correlation function of the parallel and perpendicular fluorescence intensities of T4 lysozyme single molecules shows correlated rather than anticorrelated dynamics longer than 100 μs. These results suggest that there is no rotational motion from 100 μs to seconds. Therefore, the protein either is fixed, in which case the anisotropy is determined by the related orientation of the emission dipole to the polarizer, or the protein has a rotational motion faster than 100 μs, which can be determined by the anisotropy distribution of the single molecules. Because the distribution of the emission dipoles is random among the single molecules should they be fixed, the steady-state anisotropy should have a wide distribution, ranging from -0.5 to 1.0 (Figure 2). We studied single-molecule rhodamine 123 on a PMMA surface as a control experiment of fixed molecules. No rhodamine 123 molecules show anisotropy decay dynamics (Figure 3B). The parallel intensity can be much larger than the perpendicular intensity or vice versa. The rotational fixed rhodamine 123 molecules gave anisotropy values from -0.31 (shown in Figure 3B) to 0.81 in our measurements, and the anisotropy distribution was obviously much broader compared to that of the tethered T4 lysozyme proteins on a surface under water (Figure 5). If the rotation is faster than the millisecond dwell time, both steady-state anisotropy and time zero anisotropy would show a narrow distribution because the parallel and perpendicular intensities are orientation-angle averaged. The anisotropy distribution of T4 lysozyme single molecules suggests that tethered T4 lysozyme has rotational freedom and rotates at a rate faster than 1/100 μs^{-1}. In summary, the photon delay time measurements with nanosecond time resolution show that T4 lysozyme's rotation time is about 5ns or longer (Figure 5C). The photon arrival time measurements show that tethered T4 lysozyme proteins are not fixed on a surface and essentially stay in solution.

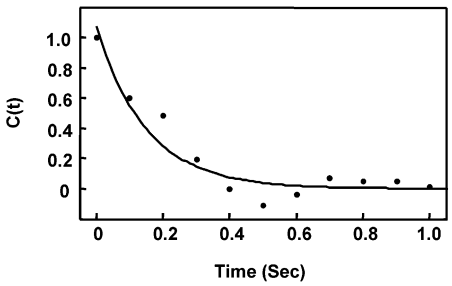

Figure 6. Autocorrelation function and single-exponential fit of the anisotropy decay rate constant trajectory of a single T4 lysozyme molecule. It shows a decay constant of 0.2 s.

We have observed that the rotational dynamics of the tethered proteins is associated with significant rate fluctuations. Figure 5 shows that the time-zero anisotropy (α) has a distribution width of 0.10 and that the anisotropy decay rate constant ($1/\rho$) has a distribution width of 0.06 ns^{-1}. On the basis of the error analysis, random error contributes to the time-zero anisotropy error of 0.01 and the decay rate error of 0.01 ns^{-1}, which are much smaller than the distribution width. The system error does not contribute to the widening of the distribution because it is the same for all single molecules. Therefore, we conclude that the distributions of the time-zero anisotropy and the anisotropy decay rate constant are due to the inhomogeneity of the single-molecule rotation dynamics. This inhomogeneity is partially due to the intrinsic rotational diffusion dynamics of tethered proteins and partially due to the probing. The spatial restriction on a tethered T4 lysozyme rotation contributes to the widening of the time-zero anisotropy distribution (as discussed in the modeling section). The proteins are attached to a surface by covalent linkage to the lysine group of the T4 lysozyme, which has 12 lysine groups in a protein. So, the bound sites are nonselective, which may cause different orientation angles, wobbling amplitudes, and angle distributions of the dye. These effects are not necessarily intrinsic to the tethered protein rotational diffusion motions. The ensemble-averaged measurements of the T4 lysozyme protein in solution show essentially the same rotation rate as the single-molecule measurement of the protein tethered on a surface under water. To investigate the existence of dynamic inhomogeneity of the rotation motion of the tethered T4 lysozyme, we calculated the autocorrelation functions of α and $1/\rho$ trajectories with a 0.1 s time-bin resolution. About 20% of the single molecules show resolvable fluctuation dynamics of α and $1/\rho$ (Figure 6) at the subsecond time scale, with a fluctuation range of about $0.2-0.4$ for α and $0.0-0.2$ ns^{-1} for $1/\rho$. The other 80% of the single molecules do not have resolvable fluctuation dynamics, suggesting that the rotational motion rate is constant for about 80% of the individual T4 lysozyme in the time scale from 0.1 s to several seconds. We postulate that the origin of the rotational rate fluctuation is due to the interactions of the tethered protein with a hydrocarbon-treated surface under water, for example, elec-

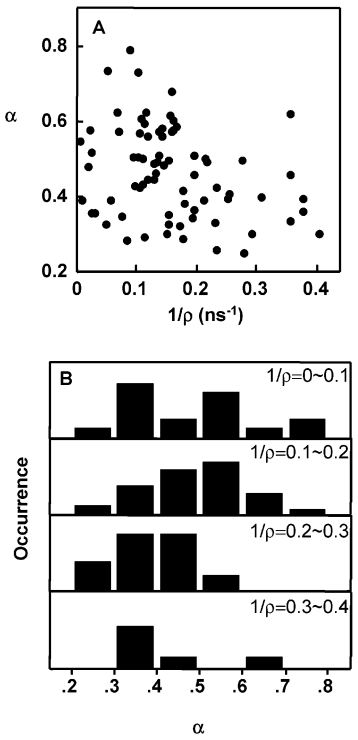

Figure 7. (A) Correlation of time-zero anisotropy (α) and anisotropy decay rate constant ($1/\rho$) from the single molecule α and $1/\rho$ trajectories. Each point corresponds to the α and $1/\rho$ values within 0.1 s bin time of the trajectory. The α and $1/\rho$ values of the full trajectories from all examined single molecules showing fluctuations are included. (B) The normalized histogram of α at different $1/\rho$ values from (A). The standard deviation of α decreases from 0.15 to 0.10 as $1/\rho$ increases from 0∼0.1 to 0.3∼0.4.

trostatic interaction and van der Waals interaction. To further verify this attribution, we analyzed the correlation of the time-zero anisotropy and decay rate constant, plotted in Figure 7A, for all molecules showing fluctuations of α and $1/\rho$. We found that the high anisotropy decay rate corresponds to a narrow distribution of α, whereas a low decay rate corresponds to a wide distribution of α (Figure 7B). For the state of T4 lysozyme contacting a surface, the rotation rate is low, with rotation possibly also restricted to a certain angular range, resulting in a wide distribution of α. On the other hand, for the state of T4 lysozyme in solution, the rotation rate is high, with the rotation reaching a half-sphere angular space and resulting in an α with a narrow distribution peaking at 0.25 ± 0.05.

The subsecond fluctuation of the anisotropy amplitude and decay rate constant of the 20% T4 lysozyme molecules suggests that (1) there are 20% of tethered T4 lysozyme proteins associated with the rotational rate fluctuation or (2) there is a 20% probability of recording the rotational rate fluctuation for a single-molecule measurement during a finite recording time, limited by single-molecule photobleaching, so that the real ratio of the tethered proteins involving in rotational rate fluctuation can be much higher than 20%. The 80% of the T4 lysozyme that does not show observed anisotropy fluctuation might still have fluctuations shorter than 0.1 s or longer than several seconds or have an amplitude too small to measure because of the S/N. Those molecules still have rotation dynamics in nanosecond or microsecond time scale but the rotation rate fluctuation is not observed. The rotation dynamics discussed here is different from rotational diffusion and jumps at millisecond time scale observed in most single molecule spectroscopy works. Although it would be extremely difficult for an ensemble-averaged experiment to distinguish between static and dynamic inhomogeneities, a single-molecule experiment can also encounter difficulties in their characterization because the anisotropy decay rate fluctuates at the comparable time scale of the measurement, which is typically limited by single-molecule photobleaching.

It is highly possible that the static inhomogeneity (Figure 5) we observed for all the single molecules examined is actually due to dynamic inhomogeneity, and the intrinsic static inhomogeneity to the overall inhomogeneity of the rotation dynamics is not significant. This conclusion is consistent with the notion that the distribution of the anisotropy in Figure 5 is mainly due to different tethering sites that give different limits for wobbling motion angles of the Alexa 488 dye molecule probes and that the local environment of the tethered single proteins is essentially homogeneous with the hydrocarbon covering of the surface. Furthermore, single tethered proteins are in solution phase without rotational rate fluctuation for most of the time during the measurements, suggesting that the rate fluctuation results from infrequent interaction of the single proteins with the surface and that the interaction has to exist generally for all tethered molecules. However, because the interaction is infrequent and transient, using tethered proteins on a modified glass surface under water is a reasonable way to study protein dynamics in solution, as many single-molecule experiments have demonstrated.[6,7]

Further application of the nanosecond anisotropy trajectories with subsecond resolution should be broad. The method is apparently applicable to probing conformation dynamics by using bifunctional dyes,[26,48] which eliminates the rotation of the probe. For example, mutant T4 lysozyme with two Cys groups at the same distance as the bifunctional dye can be labeled, and its conformation dynamics can be studied. A bifunctional fluorescent probe can be used to anchor it on the protein surface across two cystein residues so that the dye molecule self-wobbling motions are fixed and only the protein matrix motion is probed. Therefore, the interdomain and intradomain conformation dynamics of a protein can be studied by probing the fluorescent dipole rotational motion without the complication of convoluted dye motions. The nanosecond time scale protein conformational dynamics are crucial to understanding the mechanisms and dynamics of protein-folding and enzymatic reaction. Noticeably, the nanosecond single-molecule dynamics studied by single-molecule nanosecond anisotropy can be directly comparable and correlated with single-molecule dynamics from molecular dynamics simulation.

Conclusions

We studied spatially confined rotational diffusion dynamics of individual tethered proteins on a hydrocarbon modified glass surface under water using a novel approach of single-molecule nanosecond anisotropy based on previously established photon-stamping techniques. The single-molecule nanosecond anisotropy method that we have demonstrated and applied in this work has established a new approach to allow measurement of single-molecule rotational motion dynamics over a wide time range from nanoseconds to seconds. Furthermore, this approach allows the recording of time trajectories of single-molecule rotational rate constants and time-zero anisotropy amplitudes, and effectively decouples the measurement of anisotropy decay time fluctuation from that of the fluorescence lifetime fluctuation. The tethered protein rotational motions are often associated with and relevant to the protein interaction motions in the early events of cell signaling occurring on the extra- and intramembrane surfaces of living cells. Tethering proteins to the surface is also

a typical sample preparation for single-molecule spectroscopic experiments to confine single molecules under the focal spot of the laser. It is critical, then, to make a quantitative assessment of the impact on protein dynamics as proteins interact with biologically compatible surfaces. The tethered single T4 lysozyme proteins show dynamic inhomogeneity of the rotation dynamics because of their spatial confinement and their interactions with the surface, and the fluctuation of the single-molecule rotational rate constants is in a range of $0.0-0.2\ ns^{-1}$. The observed static inhomogeneity of the tethered single-protein rotation dynamics is due either to the rotation rate fluctuation at a time scale comparable to the measurement or to the inhomogeneity of the local surface and different tethering sites on the proteins. The broadness of the inhomogeneity is dependent on the linker, the surface modification, and the interaction of the protein with the surface. The proteins spend most of the time in the solution phase. The interaction between the T4 lysozyme proteins and the hydrocarbon-modified surface is weak, and the occurrence of the measurable interactions can only be observed for 20% of the molecules at no more than a few times per second. The impact of the protein−surface interactions on the protein function and dynamics is minimal or insignificant when the surface is appropriately treated to be biologically compatible.

Acknowledgment. We thank Brian Matthews for providing us with T4 lysozyme proteins, Steve Colson and Greg Harms for helpful discussions, and Gordon Anderson for help with the instrument development. This work was supported by the Chemical Sciences Division of the Office of Basic Energy Sciences within the Office of Energy Research of the U.S. Department of Energy (DOE). The Pacific Northwest National Laboratory is operated for DOE under Contract DE-AC06-76RLO1830.

References and Notes

(1) Xie, X. S.; Trautman, J. K. *Annu. Rev. Phys. Chem.* **1998**, *49*, 441.
(2) Lu, H. P.; Xun, L. Y.; Xie, X. S. *Science* **1998**, *282*, 1877.
(3) Karplus, M. *J. Phys. Chem. B* **2000**, *104*, 11.
(4) Onuchic, J. N.; Lutheyschulten, Z.; Wolynes, P. G. *Annu. Rev. Phys. Chem.* **1997**, *48*, 545.
(5) Chen, Y.; Hu, D.; Vorpagel, E. R.; Lu, H. P., submitted.
(6) Zhuang, X.; Ha, T.; Kim, H. D.; Centner, T.; Labeit, S.; Chu, S. *Proc. Natl. Acad. Sci. U.S.A.* **2000**, *97*, 14241.
(7) Edman, L.; Rigler, R. *Proc. Natl. Acad. Sci. U.S.A.* **2000**, *97*, 8266.
(8) Jia, Y. W.; Sytnik, A.; Li, L. Q.; Vladimirov, S.; Cooperman, B. S.; Hochstrasser, R. M. *Proc. Natl. Acad. Sci. U.S.A.* **1997**, *94*, 7932.
(9) Ha, T.; Ting, A. Y.; Liang, J.; Caldwell, W. B.; Deniz, A. A.; Chemla, D. S.; Schultz, P. G.; Weiss, S. *Proc. Natl. Acad. Sci. U.S.A.* **1999**, *96*, 893.
(10) Weiss, S. *Science* **1999**, *283*, 1676.
(11) Zhuang, X. W.; Bartley, L. E.; Babcock, H. P.; Russell, R.; Ha, T. J.; Herschlag, D.; Chu, S. *Science* **2000**, *288*, 2048.
(12) Moerner, W. E. *J. Phys. Chem. B* **2002**, *106*, 910.
(13) Moerner, W. E.; Orrit, M. *Science* **1999**, *283*, 1670.
(14) Tamarat, P.; Maali, A.; Lounis, B.; Orrit, M. *J. Phys. Chem. A* **2000**, *104*, 1.
(15) Schenter, G. K.; Lu, H. P.; Xie, X. S. *J. Phys. Chem. A* **1999**, *103*, 10477.
(16) Xie, X. S.; Lu, H. P. *J. Biol. Chem.* **1999**, *274*, 15967.
(17) Lu, H. P.; Iakoucheva, L. M.; Ackerman, E. J. *J. Am. Chem. Soc.* **2001**, *123*, 9184.
(18) Ha, T.; Glass, J.; Enderle, T.; Chemla, D. S.; Weiss, S. *Phys. Rev. Lett.* **1998**, *80*, 2093.
(19) Harms, G. S.; Sonnleitner, M.; Schütz, G. J.; Gruber, H. J.; Schmidt, T. *Biophys. J.* **1999**, *77*, 2864.
(20) Schutz, G. J.; Schindler, H.; Schmidt, T. *Opt. Lett.* **1997**, *22*, 651.
(21) Xie, X. S.; Dunn, R. C. *Science* **1994**, *265*, 361.
(22) Ha, T.; Enderle, T.; Chemla, D. S.; Selvin, P. R.; Weiss, S. *Phys. Rev. Lett.* **1996**, *77*, 3979.
(23) Weston, K. D.; Goldner, L. S. *J. Phys. Chem. B* **2001**, *105*, 3453.
(24) Dickson, R. M.; Norris, D. J.; Moerner, W. E. *Phys. Rev. Lett.* **1998**, *81*, 5322.
(25) Ruiter, A. G. T.; Veerman, J. A.; Garciaparajo, M. F.; Van Hulst, N. F. *J. Phys. Chem.* **1997**, *101*, 7318.
(26) Peterman, E. J. G.; Sosa, H.; Goldstein, L. S. B.; Moerner, W. E. *Biophys. J.* **2001**, *81*, 2851.
(27) Sase, I.; Miyata, H.; Ishiwata, S. I.; Kinosita, K., Jr. *Proc. Natl. Acad. Sci. U.S.A.* **1997**, *94*, 5646.
(28) Hu, D.; Yu, J.; Wong, K.; Bagchi, B.; Rossky, P. J.; Barbara, P. F. *Nature* **2000**, *405*, 1030.
(29) Deschenes, L. A.; Vanden Bout, D. A. *Science* **2001**, *292*, 255.
(30) Ha, T.; Laurence, T. A.; Chemla, D. S.; Weiss, S. *J. Phys. Chem. B* **1999**, *103*, 6839.
(31) Warshaw, D. M.; Hayes, E.; Gaffney, D.; Lauzon, A.-M.; Wu, J.; Kennedy, G.; Trybus, K.; Lowey, S.; Berger, C. *Proc. Natl. Acad. Sci. U.S.A.* **1998**, *95*, 8034.
(32) Hollars, C. W.; Dunn, R. C. *J. Chem. Phys.* **2000**, *112*, 7822.
(33) Bopp, M. A.; Sytnik, A.; Howard, T. D.; Cogdell, R. J.; Hochstrasser, R. M. *Proc. Natl. Acad. Sci. U.S.A.* **1999**, *96*, 11271.
(34) Sosa, H.; Peterman, E. J. G.; Moerner, W. E.; Goldstein, L. S. B. *Nat. Struct. Biol.* **2001**, *8*, 540.
(35) Adachi, K.; Yasuda, R.; Noji, H.; Itoh, H.; Harada, Y.; Yoshida, M.; Kinosita, K., Jr. *Proc. Natl. Acad. Sci. U.S.A.* **2000**, *97*, 7243.
(36) Mei, E.; Higgins, D. A. *J. Chem. Phys.* **2000**, *112*, 7839.
(37) Bartko, A. P.; Dickson, R. M. *J. Phys. Chem. B* **1999**, *103*, 11237.
(38) Schaffer, J.; Volkmer, A.; Eggeling, C.; Subramaniam, V.; Striker, G.; Seidel, C. A. M. *J. Phys. Chem. A* **1999**, *103*, 331.
(39) Bohmer, M.; Pampaloni, F.; Wahl, M.; Rahn, H.; Erdmann, R.; Enderlein, J. *Rev. Sci. Instrum.* **2001**, *72*, 4145.
(40) Fries, J. R.; Brand, L.; Eggeling, C.; Kollner, M.; Seidel, C. A. M. *J. Phys. Chem. A* **1998**, *102*, 6601.
(41) Zhang, X. J.; Wozniak, J. A.; Matthews, B. W. *J. Mol. Biol.* **1995**, *250*, 527.
(42) Cross, A. J.; Waldeck, D. H.; Fleming, G. R. *J. Chem. Phys.* **1983**, *78*, 6455.
(43) Cross, A. J.; Fleming, G. R. *Biophys. J.* **1984**, *46*, 45.
(44) Lakowicz, J. R. *Principles of Fluorescence Spectroscopy*, 2nd ed.; Kluwer Academic/Plenum Publishers: New York, 1999.
(45) Enderlein, J.; Erdmann, R. *Opt. Commun.* **1997**, *134*, 371.
(46) Lu, H. P.; Xie, X. S. *Nature* **1997**, *385*, 143.
(47) Cross, A. J.; Fleming, G. R. *Biophys. J.* **1986**, *50*, 507.
(48) Forkey, J. N.; Quinlan, M. E.; Goldman, Y. E. *Prog. Biophys. Mol. Biol.* **2000**, *74*, 1.